Contrasting Local and Remote Impacts of Surface Heating on Polar Warming and Amplification

KIWOONG PARK, SARAH M. KANG, AND DOYEON KIM

School of Urban and Environmental Engineering, Ulsan National Institute of Science and Technology, Ulsan, South Korea

MALTE F. STUECKER

Department of Atmospheric Sciences, University of Washington, Seattle, Washington, and Cooperative Programs for the Advancement of Earth System Science, University Corporation for Atmospheric Research, Boulder, Colorado

FEI-FEI JIN

Department of Atmospheric Sciences, School of Ocean and Earth Science and Technology, University of Hawai'i at Mānoa, Honolulu, Hawaii

(Manuscript received 8 September 2017, in final form 5 February 2018)

ABSTRACT

The polar region has been one of the fastest warming places on Earth in response to greenhouse gas (GHG) forcing. Two distinct processes contribute to the observed warming signal: (i) local warming in direct response to the GHG forcing and (ii) the effect of enhanced poleward heat transport from low latitudes. A series of aquaplanet experiments, which excludes the surface albedo feedback, is conducted to quantify the relative contributions of these two physical processes to the polar warming magnitude and degree of amplification relative to the global mean. The globe is divided into zonal bands with equal area in eight experiments. For each of these, an external heating is prescribed beneath the slab ocean layer in the respective forcing bands. The summation of the individual temperature responses to each local heating in these experiments is very similar to the response to a globally uniform heating. This allows the authors to decompose the polar warming and amplification signal into the effects of local and remote heating. Local polar heating that induces surface-trapped warming due to the large tropospheric static stability in this region accounts for about half of the polar surface warming. Cloud radiative effects act to enhance this local contribution. In contrast, remote nonpolar heating induces a robust polar warming pattern that features a midtropospheric peak, regardless of the meridional location of the forcing. Among all remote forcing experiments, the deep tropical forcing case contributes most to the polar-amplified surface warming pattern relative to the global mean, while the high-latitude forcing cases contribute most to enhancing the polar surface warming magnitude.

1. Introduction

In the polar region, surface temperatures have increased at a faster rate than the global average signal in recent decades (Hassol 2004; Hansen et al. 2006; Bekryaev et al. 2010; IPCC 2014), a phenomenon commonly referred to as polar amplification (Polyakov et al. 2002; Serreze and Francis 2006). We discuss the controlling factors of the polar amplification, as well as the absolute magnitude of polar surface warming, which will be referred to as polar warming and amplification hereafter. This polar warming and amplification is caused by local radiative processes, such as diminishing sea ice thickness and volume and the associated ice–albedo feedback (Sellers 1969; Manabe 1983; Rothrock et al. 2003; Hall 2004; Stroeve et al. 2007; Comiso et al. 2008), as well as changes in water vapor and cloud cover associated with tropospheric stability and longwave feedbacks (Francis and Hunter 2006; Winton 2006; Schweiger et al. 2008; Boé et al. 2009; Graversen and Wang 2009). Additional processes also contribute to polar warming and amplification, such as enhanced water vapor transport from low latitudes (Groves and Francis 2002; Rodgers et al. 2003) and increased cyclonic

Corresponding author: Sarah M. Kang, skang@unist.ac.kr

DOI: 10.1175/JCLI-D-17-0600.1

activity from midlatitudes (Zhang et al. 2004; Simmonds et al. 2008), which enhance atmospheric poleward energy transport (Alexeev et al. 2005; Cai 2005; Graversen et al. 2008; Graversen and Wang 2009; Yang et al. 2010; Rose et al. 2014). The attribution of individual causes is complicated by the fact that these processes occur simultaneously and interact with each other (Cai and Lu 2007; Chung and Räisänen 2011; Graversen et al. 2011; Screen et al. 2012; Kapsch et al. 2013; Feldl et al. 2017; Yoshimori et al. 2017). For example, an increase in poleward atmospheric heat transport would likely intensify sea ice melt, surface solar absorption, and heat transport from the ocean to the atmosphere (Chung and Räisänen 2011; Graversen et al. 2011; Kapsch et al. 2013), all of which would further amplify the surface warming. Therefore, it is difficult to quantify the individual contributions to polar warming and amplification between local and remote processes from observational data alone. Nevertheless, recent studies attempt to estimate the relative importance between local and remote processes that contribute to this warming signal using model simulations together with observations (Chung and Räisänen 2011; Screen et al. 2012; Yoshimori et al. 2017). It is emphasized that two distinct polar warming signatures exist, one being locally driven near-surface warming and the other characterized by mid-tropospheric warming via remote processes. However, the question of how the local and remote forcings are quantitatively different remains to be answered. It is important to note that the same magnitude of global mean radiative forcing prescribed at different locations can cause substantially different surface temperature responses (Hansen et al. 1997, 2005; Kang and Xie 2014). Furthermore, it is not clear which meridional forcing locations are most effective at warming the polar region.

The aims of this study are to decompose the effects of local and remote heating on polar warming and amplification and to quantify the relative importance of the heating depending on its meridional location. To achieve this, we utilize a similar strategy to Alexeev et al. (2005), where an atmospheric general circulation model is coupled to an aquaplanet slab ocean. Here, we prescribe anomalous heat fluxes beneath the slab ocean layer to force the atmosphere. Importantly, in our approach, the heat fluxes have smaller meridional width than in previous studies in order to compare the relative importance of each meridional forcing location on polar warming and amplification. This will allow us to distinguish between the contrasting effects of local and remote heating and estimate the relative importance of each local heating location to the vertical profile of the polar warming signal.

TABLE 1. The latitude band of prescribed surface heating for each perturbation experiment.

EXP	Forced latitude band
LOC0	7°S–7°N
LOC11	7°–15°S/N
LOC19	15°–23°S/N
LOC27	23°–31°S/N
LOC35	31°–39°S/N
LOC44	39°–49°S/N
LOC55	49°–61°S/N
LOC75	61°–90°S/N
GLO	90°S–90°N

2. Model and experimental setup

We employ the atmospheric general circulation model developed at the Geophysical Fluid Dynamics Laboratory (GFDL), AM2 (Anderson et al. 2004). The model has a horizontal resolution of 2° latitude × 2.5° longitude and 24 vertical levels. The atmosphere is coupled to an aquaplanet slab ocean with a heat capacity of 2×10^8 $\mathrm{J\,K^{-1}\,m^{-2}}$, corresponding to an ocean mixed layer depth of 50 m. The sea surface temperatures (SSTs) are permitted to drop below the freezing temperature without forming any sea ice, thus inhibiting the surface albedo feedback. The model is forced by an annual mean solar insolation (eccentricity = 0; obliquity = 23.5°) without a diurnal cycle.

To investigate the local and remote impacts on polar warming and amplification, the control climate with no heat flux adjustment (CNT) is perturbed by a series of experiments with zonally symmetric surface heating prescribed over finite latitude bands that are symmetric about the equator (Table 1). The model and experiment setup are the same as in Kang et al. (2017). The time-constant surface heating is linearly tapered to zero within two grid points at both lateral boundaries. The maximum amplitude of forcing is set to $4\,\mathrm{W\,m^{-2}}$, which is the approximate radiative forcing for a CO_2 doubling (Hansen et al. 1997). We also conduct the same suite of experiments but with a negative forcing of $4\,\mathrm{W\,m^{-2}}$ in order to obtain a linear climate response, which is computed as the difference of the responses to heating and cooling divided by a factor of 2. All figures herein indicate the linear component averaged between the two hemispheres since the climate is hemispherically symmetric in our experiment setup. The perturbation experiments with localized heating (LOC) are denoted as LOC#, with # denoting the center of the forced latitude band. For example, LOC35 indicates the experiment for which the surface heating is prescribed over 31°–39° latitude in both hemispheres. We conduct eight LOC experiments in total, constraining the area of the

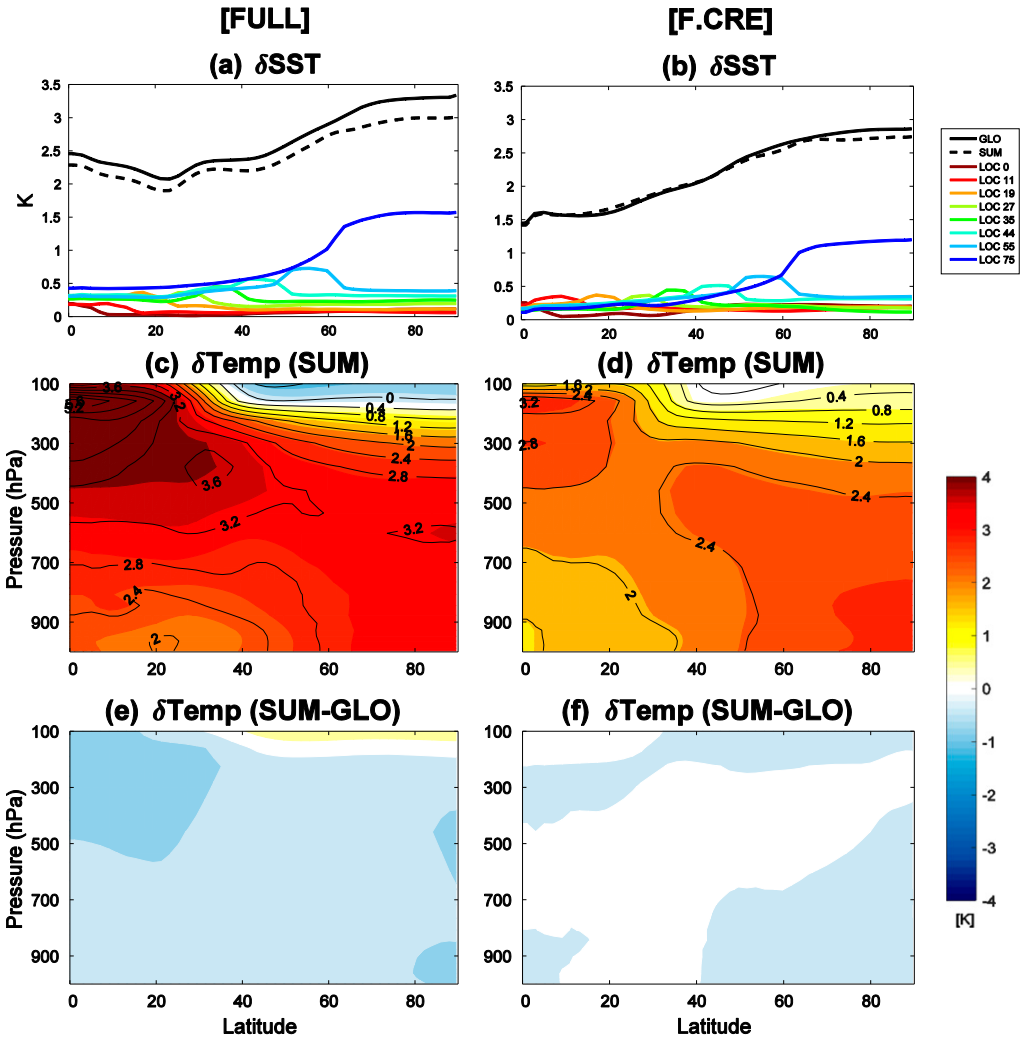

FIG. 1. The zonal-mean response of (a),(b) SST (K) in GLO (black solid line), SUM (black dashed line), and LOC# (colored solid lines); (c),(d) air temperature (K; an interval of 0.4 K) in SUM (shading) and GLO (contours); and (e),(f) the difference between SUM and GLO. (a),(c),(e) FULL and (b),(e),(f) F.CRE. All values are anomalies relative to the respective control (CNT) climate.

forced latitude band in each LOC to be approximately the same to allow for equal comparisons. An additional perturbation experiment with globally uniform heating is denoted as GLO. If the climate system is completely linear, the GLO response would be identical to the sum of all LOC responses, denoted as SUM.

We conducted the same set of experiments with cloud radiative effects (CRE) inhibited as in Kang et al. (2008) to understand the effects of cloud radiative feedbacks on polar warming and amplification. The time-varying cloud radiative properties are obtained from the CNT experiment and repeated annually in the fixed cloud model (F.CRE), which results in the control climatology being very similar between the default and the fixed cloud model. The default model with all dynamics included is referred to as FULL and the fixed cloud model as F.CRE. The CNT experiment is integrated for 120 years, and the average of the last 100 years is analyzed. The perturbation experiments that are branched out from an equilibrated CNT state are integrated for 60 years, and the first 15 years are discarded as spinup period.

3. Results

a. *Linearity of the climate response*

A comparison of the anomalous (with regard to CNT) zonal-mean SST responses in GLO (solid black line) and SUM (dashed black line) in the default model (FULL) is shown in Fig. 1a. The SST response in SUM closely reproduces the GLO response as a function of latitude,

albeit with a reduced magnitude. In terms of the global mean SST response, SUM underestimates GLO by less than 7%, thereby demonstrating that the SST response is highly linear. Furthermore, the tropospheric temperature response for SUM (Fig. 1c) is only slightly weaker than the GLO response at all latitudes throughout the troposphere (Fig. 1e). The small nonlinear component partially originates from radiative effects of cloud fraction changes, which is demonstrated by the more linear response in the fixed cloud (F.CRE) experiment for both the SST (Fig. 1b) and the tropospheric temperatures (Figs. 1d–f). In FULL, the reduced tropical tropospheric warming in SUM, compared to GLO (Fig. 1e), is due to a larger reduction of high-level clouds in the tropics in SUM (Fig. 2a). This results from the Clausius–Clapeyron (CC) relation, which causes the specific humidity increases in SUM to be smaller than those in GLO. Assuming a constant relative humidity, one can estimate the specific humidity increase for the tropospheric temperature response in SUM using the CC relation [i.e.,$q(T_{\mathrm{CNT}}+\delta T_{\mathrm{SUM}})-q(T_{\mathrm{CNT}})$]. The actual specific humidity response in SUM (i.e., δq_{SUM}) is always smaller than the value obtained from the CC relation (i.e., δq_{CC}) because the saturation specific humidity increases exponentially with temperature (Fig. 2b). The difference is largest in the warm tropics and decreases both with latitude and altitude. Hence, the tropics are substantially drier in SUM, compared to GLO (Fig. 2c), which leads to a larger reduction of high-level clouds in the former (Fig. 2a). This explains a more linear climate response in the F.CRE experiments, compared to the default model (FULL). This effect is, however, relatively small; thus, both FULL and F.CRE exhibit a near-linear response (Fig. 1), which justifies a decomposition of the climate response into local and remote effects.

b. *Local versus remote impacts on polar warming and amplification*

Despite an absence of surface albedo feedback, the surface warming in both GLO and SUM features a polar amplified pattern regardless of CRE (Figs. 1a–d), consistent with previous studies (Alexeev et al. 2005; Cai 2005; Graversen and Wang 2009; Yang et al. 2010; Kang and Xie 2014; Rose et al. 2014). As we demonstrated a near-linearity of the response, we are able to decompose the polar warming and amplification signal into the contribution from polar (LOC75) and nonpolar (sum of the remainder) forcing, which respectively represents the local and remote effects (Figs. 3, 4). First, we compare the relative contributions of polar (solid lines) and

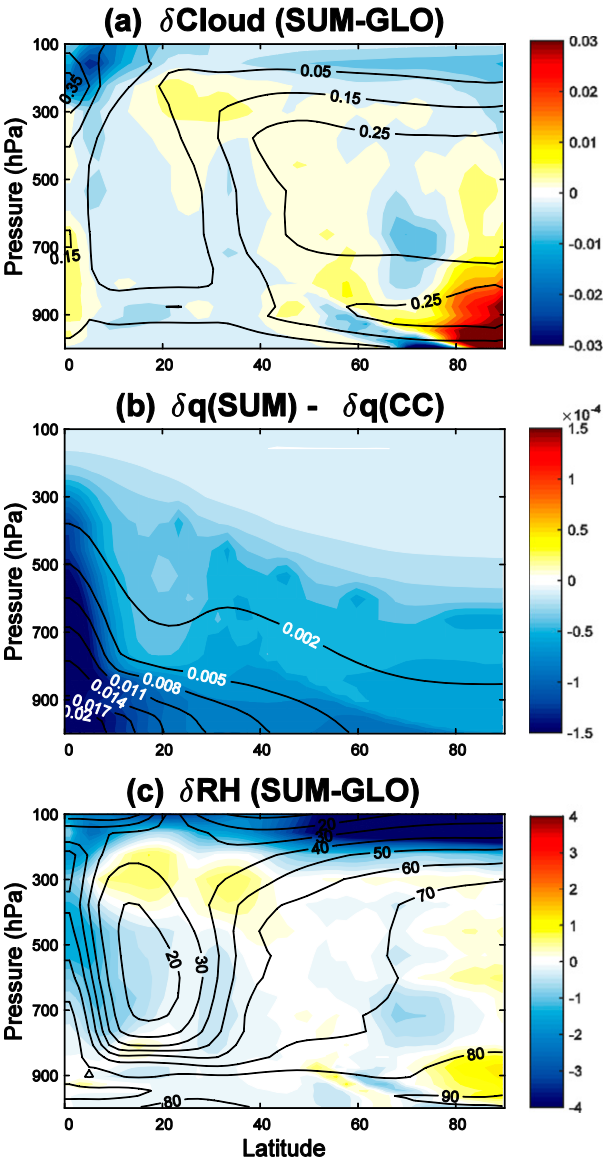

FIG. 2. The zonal-mean (a) cloud amount fraction difference between SUM and GLO (shading; with an interval of 0.003), (b) specific humidity in SUM minus the specific humidity change obtained from the CC relationship (shading; with an interval of $10^{-5}\,\mathrm{g\,kg^{-1}}$), and (c) relative humidity difference between SUM and GLO (shading; with an interval of 0.2%). The contour lines in all panels indicate the CNT profile for each variable with an interval of (a) 0.1, (b) $3\times10^{-3}\,\mathrm{g\,kg^{-1}}$, and (c) 10%.

nonpolar (dashed lines) forcing to the SST response in FULL (red lines in Fig. 3a). Nearly 50% of the polar surface warming, defined as the average warming poleward of 60°, results from the polar forcing in FULL (solid red line, Fig. 3a). The contribution by polar forcing on polar region is far greater than the fraction expected for a completely diffusive climate system where the response is nearly isothermal, in which case the

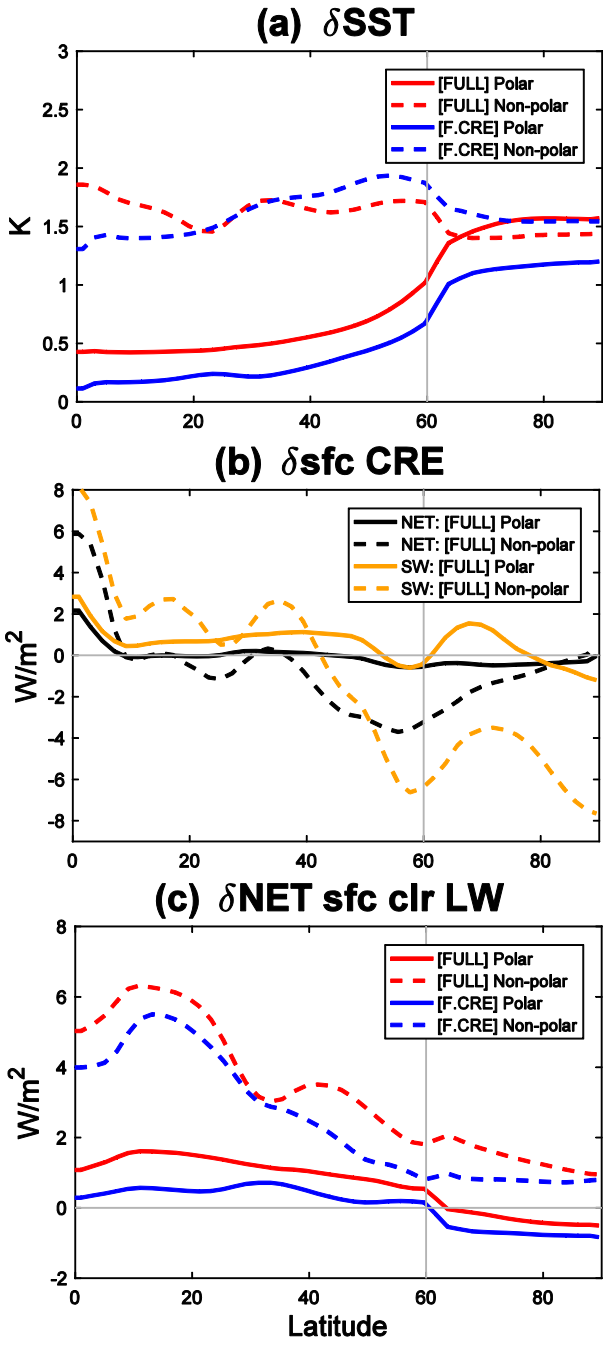

FIG. 3. The zonal-mean response of (a) SST (K), (b) net (black) and shortwave (orange) cloud radiative effects at the surface ($W\,m^{-2}$), and (c) clear-sky downward longwave radiation at the surface ($W\,m^{-2}$) in FULL (red lines) and F.CRE (blue lines). In all panels, the solid lines indicate the local polar contribution (LOC75), and the dashed lines indicate the remote nonpolar contribution (SUM-LOC75). In (b) and (c), positive values indicate downward fluxes.

fraction of local effect would merely be the area fraction of forced latitude band (i.e., 1/8). This is suggestive of a positive feedback that amplifies the effect of the polar forcing, such as the lapse rate feedback (Pithan and Mauritsen 2014). In contrast, the surface warming response outside of the polar region (e.g., equatorward of 60°) exhibits a significantly larger contribution from the local forcing than the forcing outside the forced latitude band, where the outside forcing contributes from 63% to 92% to local surface warming. In particular, the polar heating (LOC75) experiment exhibits the largest contribution to warming the surface of the entire globe (Figs. 1a,b). Thus, the dominance of the local contribution is an intrinsic characteristic of polar surface warming. This is due to the large atmospheric static stability in the polar region that traps the warming response near the surface, thereby amplifying the local effect (Figs. 4a,b) (Graversen et al. 2014; Kang and Xie 2014; Pithan and Mauritsen 2014). In contrast, the maximum warming response to local forcing in other regions (e.g., the response of equatorward of 60° in LOC0 ~ LOC55) occurs in the mid-to-upper troposphere, thereby degrading the local contribution (Figs. 4d,e).

The local contribution to polar surface warming decreases from 50% in FULL to 40% in F.CRE (Fig. 3a). When investigating the tropospheric temperature response, we clearly observe that polar warming is maximized near the surface in response to polar forcing (Figs. 4a,b), as opposed to the maximized warming response in the midtroposphere (at around 500 hPa) to nonpolar forcing (Figs. 4d,e) in both FULL and F.CRE. The contrasting vertical structures of polar warming for polar and nonpolar forcing result in an opposite response in the low cloud amount to these different forcings. The surface-trapped warming in LOC75 results in a decrease of the lower-tropospheric static stability, thus leading to a reduction of low cloud amount in the polar region (Fig. 4c), which acts to warm the polar surface via increased net shortwave flux (solid orange line, Fig. 3b). Hence, allowing CRE (i.e., FULL) enhances the contribution of polar forcing to the polar surface warming. In contrast, the maximized warming in the midtroposphere in response to nonpolar forcing (e.g., SUM minus LOC75) results in a moistening of the upper troposphere and thus increases the lower-tropospheric static stability. Consequently, the cloud amount increases in the polar upper and lower troposphere (Fig. 4f), which acts to cool the polar surface via enhanced shortwave reflection (dashed orange line, Fig. 3b). Hence, the active CRE (i.e., FULL) damps the contribution of nonpolar forcing to polar surface warming. Note that the quantitative assessment of the contribution of nonpolar forcing to polar surface warming is model dependent

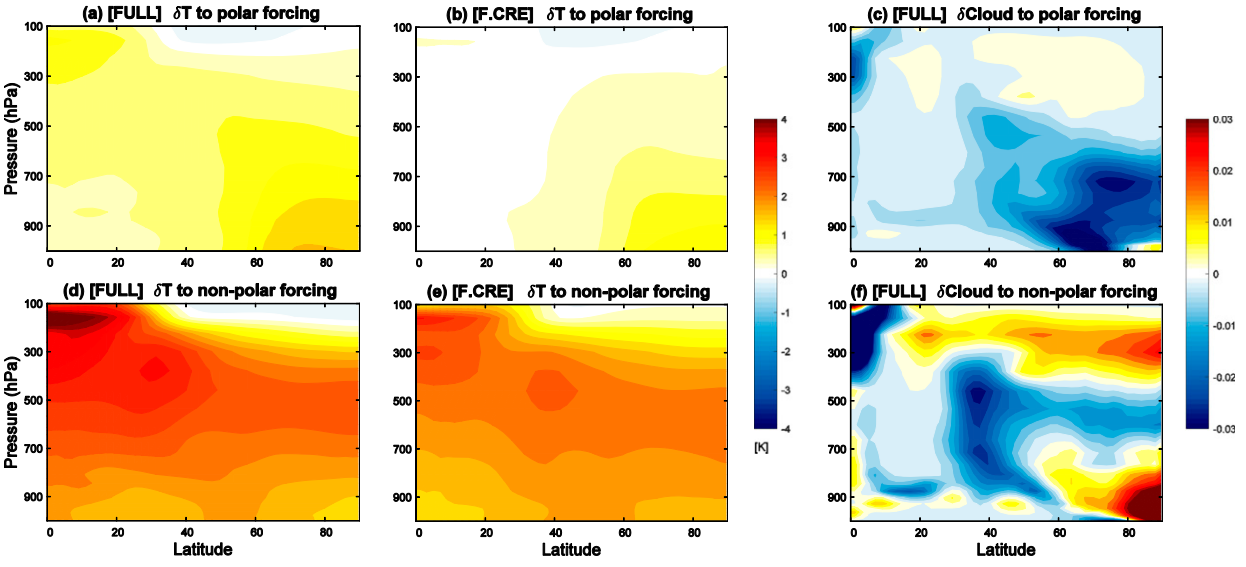

FIG. 4. The zonal-mean temperature response (K; shading with an interval of 0.4 K) for LOC75 (i.e., local polar contribution) in (a) FULL and (b) F.CRE. (c) The zonal-mean cloud amount response (fraction; shading with an interval of 0.003) for LOC75 in FULL. (d)–(f) As in (a)–(c), but for SUM-LOC75 (i.e., remote nonpolar contribution).

and that the model used in this study exhibits a relatively large shortwave cloud radiative feedback over high latitudes, compared to other models (Andrews et al. 2012; Rose et al. 2014). However, the dynamical mechanism proposed here to explain the response of the atmosphere to nonpolar forcing should be robust and not model dependent, given that it is consistent with Yoshimori et al. (2017). In the next section, we investigate the mechanisms by which nonpolar forcing induces the polar warming and amplification and attempt to identify the most efficient region for warming the polar surface.

c. *Impact of nonpolar forcing on polar warming and amplification*

As shown in Fig. 3a, 50% (60%) of the polar surface warming results from nonpolar forcing in FULL (F.CRE). It is worth noting that the nonpolar forcing induces a warming pattern with a rather flat meridional surface temperature gradient (dashed lines, Fig. 3a). This indicates that nonpolar forcing itself contributes much less to the polar-amplified surface temperature response than local polar forcing; instead, it amplifies the warming more uniformly. This is in contrast with Yoshimori et al. (2017), where the nonpolar forcing induces a greater polar warming and amplification than the local polar forcing. The nonpolar-forcing-induced polar tropospheric temperature responses in Yoshimori et al. (2017) exhibit a surface-trapped pattern rather than a midtropospheric peak, as in our experiments. The contrast is potentially due to the use of annual mean insolation and the absence of surface albedo feedback in our study, which diminishes the near-surface static stability in the polar region, thereby constituting a weakening of the lapse rate feedback (Kim et al. 2017, manuscript submitted to *J. Climate*). Thus, it demonstrates that the remote nonpolar impact itself is also modulated by local radiative feedbacks.

In our experiments, the degree of polar amplification, obtained by dividing the SST changes in the polar region by the global mean, ranges from 0.55 to 1.61 (0.75 to 1.58) in response to nonpolar forcing and is 2.26 (2.9) in response to polar forcing in FULL (F.CRE). The sum of nonpolar forcing experiments (dashed lines in Fig. 3a) produces the index of 0.88 (1.00). It is worth noting that among all nonpolar forcing cases (i.e., LOC0 ~ LOC55), the LOC0 experiment, which shows an enhancement of the rising branch of the zonal-mean Hadley circulation, exhibits the largest degree of polar amplification, which is 1.61 (1.58). The zonal-mean SST response pattern in the LOC0 experiment resembles the change of downwelling longwave radiation pattern in both FULL and F.CRE. This implies that deep tropical forcing can effectively warm the polar region with amplification, despite the distance from the pole, by enhancing the mean atmospheric circulation and water vapor transport (Schneider et al. 1997; Rodgers et al. 2003). However, note that this large polar amplification index arises partly due to the small global mean warming response in LOC0. For reference, the LOC0 experiment produces a polar surface warming of 0.1 K, equivalent to the one in the LOC19 experiment and 25% of the one in the LOC55 experiment.

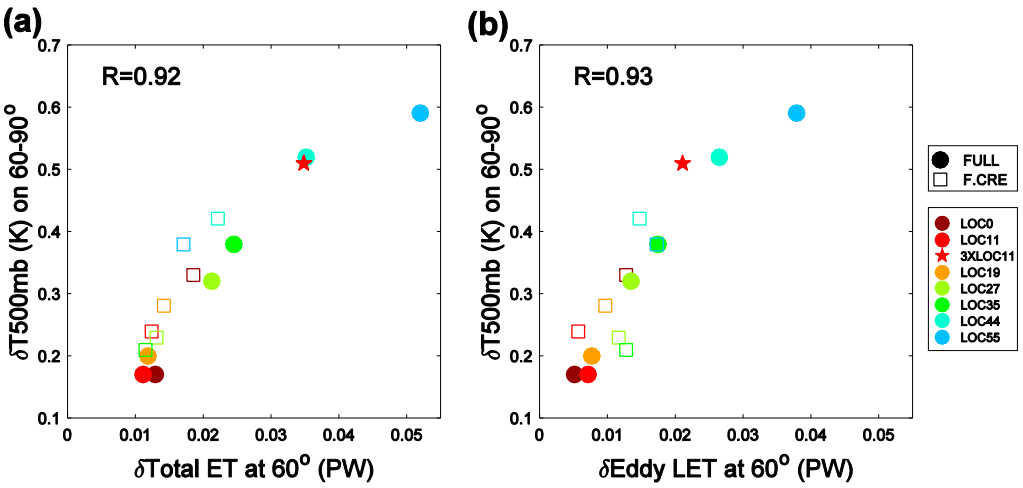

FIG. 5. Scatterplot of the 500-hPa temperature response (K) averaged over 60°–90° vs (a) the total atmospheric energy transport response across 60° (PW) and (b) the eddy latent energy transport response across 60° (PW) in FULL (closed circles) and F.CRE (open squares). The red stars indicate the response in a FULL LOC11 sensitivity experiment with the forcing amplitude multiplied by a factor of 3 (3xLOC11).

The nonpolar forcing contributes to polar surface warming via increases in downward longwave radiation at the surface (dashed lines in Fig. 3c). Note that we show the net (i.e., down − up) radiation instead of only the downwelling component to emphasize when the positive greenhouse effect (changes in downwelling longwave radiation) overcomes the negative Planck feedback (changes in upwelling longwave radiation). In contrast, the local polar forcing induces the anomalous surface longwave radiation of opposite sign (solid lines in Fig. 3c). This contrast results from the differences in the vertical profile of the temperature response. The remote nonpolar-forcing-induced polar warming exhibits a maximum in the midtroposphere (Figs. 4d,e), whereas the local polar forcing induces a bottom-heavy warming profile in the polar region (Figs. 4a,b). The tendency of increasing downward surface longwave radiation in response to nonpolar forcing appears in both FULL and F.CRE, but there is a larger increase in FULL than in F.CRE (red vs blue lines in Fig. 3c), despite a larger remote nonpolar contribution in F.CRE (Fig. 3a). This is because the effects of the net clear-sky longwave radiation in FULL are more than offset by an increased shortwave reflection by clouds (dashed orange in Fig. 3b).

Then, the question arises as to how the nonpolar forcing induces the maximized midtropospheric polar warming. A possible mechanism is an increase of atmospheric poleward heat and moisture transport, as proposed in previous studies (Schneider et al. 1997; Rodgers et al. 2003; Alexeev et al. 2005; Graversen et al. 2008; Yang et al. 2010; Chung and Räisänen 2011; Alexeev and Jackson 2013). Indeed, the anomalous atmospheric poleward energy transport across 60° is highly correlated with the 500-hPa temperature response averaged over 60°–90° ($R = 0.92$, obtained from a combination of FULL and F.CRE; Fig. 5a). The enhanced total poleward energy transport is mainly accomplished by the increased poleward eddy latent energy transport (Fig. 5b). A larger increase in the poleward eddy latent energy transport arises in the experiments where a larger SST warming is induced locally, that is, within the forced latitude band. For example, a strong correlation ($R = 0.82$, obtained from a combination of FULL and F.CRE) exists between the absolute magnitude of SST warming in the respective forced latitude band in each LOC experiment (i.e., local SST change) and the corresponding anomalous eddy latent energy transport across 60°. In general, the local SST change increases in magnitude for a higher-latitude forcing, which can be explained by cloud radiative and temperature feedbacks (both Planck and lapse rate feedback), as seen in Fig. 6b (Kang and Xie 2014; Pithan and Mauritsen 2014; Seo et al. 2014). The Planck feedback, which is associated with vertically uniform warming, requires a larger warming at colder background temperatures to balance the prescribed surface heating. In contrast, the lapse rate feedback is connected to the vertical structure of atmospheric warming. The top-heavy warming profile in the tropics gives rise to a negative lapse rate feedback, while a bottom-heavy profile in the polar region gives rise to a positive lapse rate feedback. Moreover, cloud radiative effects tend to be more positive for higher-latitude forcing in the model

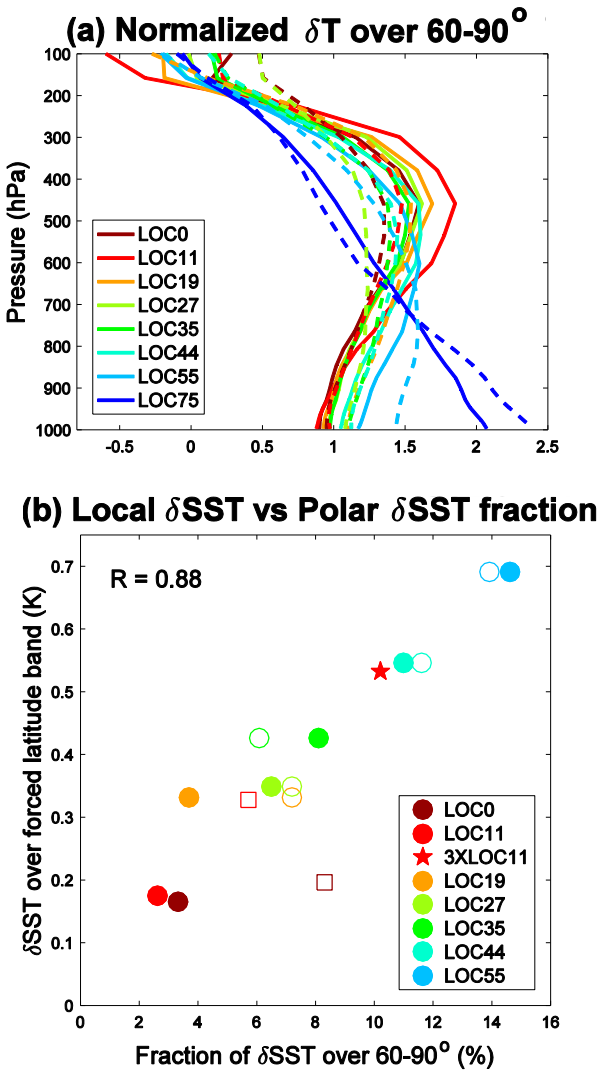

FIG. 6. (a) The vertical profiles of the air temperature responses averaged over 60°–90° divided by their vertical mean value for each experiment in FULL (solid) and F.CRE (dashed) and (b) the scatterplot of the SST response averaged over 60°–90° divided by that in SUM vs the SST response averaged over forced latitude band of LOC# for FULL (closed circles) and F.CRE (open squares). The red star in (b) indicates the response in 3xLOC11.

used in this study (Kang et al. 2008). Hence, the magnitude of local SST change is a function of the latitude location of forcing.

These results indicate that the magnitude of local SST change sets the magnitude of the surface and midtroposphere responses in the polar region and that the latitude location of forcing merely determines this magnitude. To test this hypothesis, we run a sensitivity experiment in which we apply a forcing in LOC11 with 3 times the regular amplitude (3xLOC11) to generate a local SST change that is of similar magnitude to that in the regular LOC44 experiment. That is, the SST change over 7°–15° in 3xLOC11 is of similar magnitude to that over 39°–49° in LOC44 (which can be confirmed from Fig. 6b). The red stars in Figs. 5a and 5b show the polar 500-hPa temperature response in the 3xLOC11 experiment against the total atmospheric energy transport response across 60° and the eddy latent energy transport response across 60°, respectively. We find that the scaling is nearly linear, where the response in the 3xLOC11 experiment is about 3 times as large as in the LOC11 experiment and of similar magnitude as in the LOC44 experiment. The latent energy transport by mean circulation, in contrast, is less effective because of a strong cancellation by the dry static energy transport by mean circulation (Held and Soden 2006; Yoshimori et al. 2017). The correlation coefficient between the mean latent energy transport across 60° and the 500-hPa temperature response averaged over 60°–90° is only −0.13 (when FULL and F.CRE are combined). This is consistent with earlier studies that suggest the increased eddy latent energy transport induces the midtropospheric warming in the polar region (Chung and Räisänen 2011; Feldl et al. 2017).

One may expect that the more effective the meridional forcing location is at producing the midtropospheric polar warming, the more amplified the polar surface warming will be. To better establish the relationship between the meridional location of prescribed surface heating and the anomalous vertical temperature profile in the polar region, we plot the vertical profiles of the air temperature response averaged over 60°–90° divided by their vertical mean value for each experiment (Fig. 6a). We notice a common feature among these responses to nonpolar forcing (i.e., LOC0 ~ LOC55) and a distinctly different response to polar forcing (LOC75). The peak of warming in the nonpolar forcing experiments exists in the midtroposphere and is insensitive to whether CRE is active or not (FULL vs F.CRE), although we observe small differences in the exact level where the warming peak is located between each LOC#. This indicates that a similar high-latitude temperature response pattern emerges regardless of the meridional location of remote forcing (Kang et al. 2017), suggesting the robustness of the midlevel amplified warming in the polar region in response to nonpolar forcing.

Since the area-weighted magnitude of prescribed surface heating is constrained to be equal in all LOC experiments, we can clearly quantify the contribution of each local heating to the polar surface warming. In FULL (closed circles in Fig. 6b), the closer the forcing is located to the pole, the larger the polar surface warming is. For example, LOC0 accounts for 3% of total polar surface warming, but LOC55 accounts for 15% of it. This is because the SST response in the respective forced

latitude band in LOC experiments gradually increases with the latitude at which the same forcing is applied, as suggested by a strong correlation of 0.88 (FULL and F.CRE combined) between the fractional contribution to polar surface warming and the surface warming magnitude in the respective forced latitude band (Fig. 6b). In F.CRE (open squares in Fig. 6b), the forcing locations close to the pole still effectively warm the polar surface (e.g., LOC44 = 12% and LOC55 = 14%). However, the low-latitude forcing cases in F.CRE (LOC0 ~ LOC19) become more effective at warming the polar region as compared with FULL because these cases exhibit a larger SST response in the forced latitude band in F.CRE than in FULL due to a negative CRE at the surface locally (not shown). Therefore, in general, the higher-latitude forcing is more efficient in causing the polar surface warming because a larger SST response is induced in the forced latitude band.

Thus, a larger local SST response in the forced latitude band will lead to an increased poleward eddy latent energy transport. This in turn will cause enhanced midtropospheric warming in the polar region. Furthermore, an increase of downward longwave radiation will lead to larger polar surface warming.

4. Conclusions and discussion

In this study, we contrast impacts of local and remote surface forcing on polar warming and amplification. A comprehensive series of idealized experiments is utilized to decompose the response to a globally uniform heating into the impacts from localized heating at different latitudinal bands. The polar warming in response to local polar forcing is trapped near the surface due to the large atmospheric static stability, whereas the response to remote nonpolar forcing features a maximum warming in the polar mid-to-upper troposphere. This contrasting vertical warming response profile to polar and nonpolar forcing makes the local component particularly important for the polar surface amplified warming because the bottom-heavy warming is amplified by the lapse rate feedback (Kang and Xie 2014; Pithan and Mauritsen 2014). In fact, the sum of nonpolar forcing experiments induces a warming pattern with a rather flat meridional surface temperature gradient. This implies that without local coupled feedbacks, such as the surface albedo feedback, remote processes solely cannot be invoked to explain polar surface warming and amplification, except for deep tropical forcing with an enhanced zonal-mean circulation (Schneider et al. 1997; Rodgers et al. 2003). Note that the deep tropical forcing induces a polar amplified warming pattern, but its contribution to the absolute magnitude of polar warming is small.

The nonpolar forcing induces a polar surface warming via increases in the downward longwave radiation at the surface, which results from the maximized midtropospheric polar warming. Regardless of the forcing location, the nonpolar forcing is shown to cause a polar warming maximized in the midtroposphere. This midtropospheric polar warming peak in response to nonpolar forcing is an intrinsic characteristic of atmospheric dynamics (Yoshimori et al. 2017), resulting from an increase of atmospheric poleward energy transport, mainly accomplished by an enhanced eddy latent energy transport. Recently, Graversen and Burtu (2016) showed (based on reanalysis and model data) that increased eddy latent energy transport is mostly explained by planetary-scale waves and only to a lesser degree by synoptic-scale waves. These planetary-scale waves act to warm the polar region via an enhancement of the greenhouse effect, which implies that the vertical structure of polar warming seen in our idealized experiment is realistic. In addition, the role of the latent heating by eddy flux for inducing the midtropospheric warming in the polar region has been noted by previous studies (Chung and Räisänen 2011; Feldl et al. 2017; Yoshimori et al. 2017). The nonpolar forcing that produces a larger SST warming locally gives rise to a larger response of poleward eddy latent energy transport (e.g., when comparing the response in 3xLOC11 vs LOC44), thereby leading to a larger polar warming in the midtroposphere, as well as at the surface. A larger local SST response occurs as the forcing is prescribed at higher latitudes due to the Planck and lapse rate feedbacks (Pithan and Mauritsen 2014; Seo et al. 2014). Therefore, the higher-latitude forcing is more effective at warming the polar surface.

In the current literature, there is a debate on the roles of atmospheric heat transport (AHT) and local feedbacks in their relative contribution to polar warming and amplification. In fully coupled GCMs, the polar warming and amplification are negatively correlated with the change of atmospheric heat transport (δAHT) due to the reduced meridional temperature gradient in the lower troposphere. Instead, the multimodel spread of polar warming and amplification is better explained by model differences of the surface albedo feedback (Hwang et al. 2011). In addition, Kay et al. (2012) showed that local surface albedo feedback, rather than δAHT, can explain most of the difference in polar warming and amplification between CAM4 and CAM5. In contrast, Kim et al. (2017, manuscript submitted to *J. Climate*) demonstrated that AHT can contribute to polar warming and amplification in idealized simulations with no surface albedo feedback. Even under the existence of surface albedo feedback, studies that used a

simple box model suggested that AHT can contribute to polar warming and amplification (Cai 2005; Cai and Lu 2007; Alexeev and Jackson 2013). In the modeling studies attempting to contrast the local and remote contribution to the polar warming and amplification, the remote forcing effect is suggested to be predominant (Chung and Räisänen 2011; Screen et al. 2012; Yoshimori et al. 2017). However, it is difficult to disentangle the relative importance of local radiative feedback and AHT to polar warming and amplification because of their tight interactions (Kim et al. 2017, manuscript submitted to *J. Climate*). Further complications arise from the fact that AHT and local radiative feedbacks (e.g., cloud and surface albedo) are both sensitive to model physics (Crook et al. 2011) and seasonality (Lu and Cai 2009; Yoshimori et al. 2014, 2017; Kim et al. 2017, manuscript submitted to *J. Climate*). Despite these seemingly conflicting results, one can find the common feature that strong local feedback (e.g., surface albedo response) in the polar region acts to diminish the effect of AHT through reducing the dry static energy component. This common feature is revealed in our experiments: the nonpolar forcing accounts for 50% (60%) of total polar surface warming in FULL (F.CRE) with increasing AHT but induces no polar amplification, except for the deep tropical forcing experiment (LOC0). The polar forcing accounts for the rest of the total polar warming with decreasing AHT that induces stronger polar amplification than nonpolar forcing does. These results demonstrate that local and remote forcings give rise to distinct polar warming and amplification patterns due to the contrasting vertical structure of polar warming response to these two classes of forcing.

Using similar model experiments with inhibited CRE, we show that CREs amplify the polar surface warming in response to polar forcing. The surface-trapped warming in response to polar forcing results in a reduction of low cloud amount in the polar region, which in turn leads to an increased net shortwave flux. In contrast, the maximized warming in the midtroposphere in response to nonpolar forcing results in an increase of lower-tropospheric cloud amount in the polar region, which in turn leads to increased shortwave reflection. Hence, the CRE acts to amplify the effect of polar forcing on the polar surface warming while damping the effect of nonpolar forcing on polar surface warming. The magnitude of CRE can be varied by season, as longwave CRE has a dominant role on polar warming in late autumn to early winter (Yoshimori et al. 2014, 2017). However, the suggested role of CRE in this dynamical mechanism should exist also (albeit weaker) in the annual mean.

The experimental configuration utilized in this study can serve as a test bed to compare the climatic impacts of local and remote heating in a wide range of GCMs. This type of model intercomparison study could be very useful in helping to identify the regions that are most responsible for the multimodel spread seen in the current generation of complex climate models for climate feedbacks and climate sensitivity.

Acknowledgments. We are very grateful for constructive and valuable comments and suggestions made by three anonymous reviewers. S.M.K., K.P., and D.K. were supported by Basic Science Research Program through the National Research Foundation of Korea (NRF) funded by the Ministry of Science, ICT and Future Planning (2016R1A1A3A04005520). M.F.S. was supported by the NOAA Climate and Global Change Postdoctoral Fellowship Program, administered by UCAR's Cooperative Programs for the Advancement of Earth System Sciences (CPAESS). The model data in this study can be obtained at https://github.com/UNISTkwpark/UNIST_CDL_POLAR_AMP. The authors declare no conflict of interest.

REFERENCES

Alexeev, V. A., and C. H. Jackson, 2013: Polar amplification: Is atmospheric heat transport important? *Climate Dyn.*, **41**, 533–547, https://doi.org/10.1007/s00382-012-1601-z.

——, P. L. Langen, and J. R. Bates, 2005: Polar amplification of surface warming on an aquaplanet in "ghost forcing" experiments without sea ice feedbacks. *Climate Dyn.*, **24**, 655–666, https://doi.org/10.1007/s00382-005-0018-3.

Anderson, J. L., and Coauthors, 2004: The new GFDL global atmosphere and land model AM2–LM2: Evaluation with prescribed SST simulations. *J. Climate*, **17**, 4641–4673, https://doi.org/10.1175/JCLI-3223.1.

Andrews, T., J. M. Gregory, M. J. Webb, and K. E. Taylor, 2012: Forcing, feedbacks and climate sensitivity in CMIP5 coupled atmosphere-ocean climate models. *Geophys. Res. Lett.*, **39**, L09712, https://doi.org/10.1029/2012GL051607.

Bekryaev, R. V., I. V. Polyakov, and V. A. Alexeev, 2010: Role of polar amplification in long-term surface air temperature variations and modern Arctic warming. *J. Climate*, **23**, 3888–3906, https://doi.org/10.1175/2010JCLI3297.1.

Boé, J., A. Hall, and X. Qu, 2009: Current GCMs' unrealistic negative feedback in the Arctic. *J. Climate*, **22**, 4682–4695, https://doi.org/10.1175/2009JCLI2885.1.

Cai, M., 2005: Dynamical amplification of polar warming. *Geophys. Res. Lett.*, **32**, L22710, https://doi.org/10.1029/2005GL024481.

——, and J. Lu, 2007: Dynamical greenhouse-plus feedback and polar warming amplification. Part II: Meridional and vertical asymmetries of the global warming. *Climate Dyn.*, **29**, 375–391, https://doi.org/10.1007/s00382-007-0238-9.

Chung, C. E., and P. Räisänen, 2011: Origin of the Arctic warming in climate models. *Geophys. Res. Lett.*, **38**, L21704, https://doi.org/10.1029/2011GL049816.

Comiso, J. C., C. L. Parkinson, R. Gersten, and L. Stock, 2008: Accelerated decline in the Arctic sea ice cover. *Geophys. Res. Lett.*, **35**, L01703, https://doi.org/10.1029/2007GL031972.

Crook, J. A., P. M. Forster, and N. Stuber, 2011: Spatial patterns of modeled climate feedback and contributions to temperature response and polar amplification. *J. Climate*, **24**, 3575–3592, https://doi.org/10.1175/2011JCLI3863.1.

Feldl, N., B. T. Anderson, and S. Bordoni, 2017: Atmospheric eddies mediate lapse rate feedback and Arctic amplification. *J. Climate*, **30**, 9213–9224, https://doi.org/10.1175/JCLI-D-16-0706.1.

Francis, J. A., and E. Hunter, 2006: New insight into the disappearing Arctic sea ice. *Eos, Trans. Amer. Geophys. Union*, **87**, 509–511, https://doi.org/10.1029/2006EO460001.

Graversen, R. G., and M. H. Wang, 2009: Polar amplification in a coupled climate model with locked albedo. *Climate Dyn.*, **33**, 629–643, https://doi.org/10.1007/s00382-009-0535-6.

——, and M. Burtu, 2016: Arctic amplification enhanced by latent energy transport of atmospheric planetary waves. *Quart. J. Roy. Meteor. Soc.*, **142**, 2046–2054, https://doi.org/10.1002/qj.2802.

——, T. Mauritsen, M. Tjernström, E. Källén, and G. Svensson, 2008: Vertical structure of recent Arctic warming. *Nature*, **451**, 53–56, https://doi.org/10.1038/nature06502.

——, ——, S. Drijfhout, M. Tjernström, and S. Mårtensson, 2011: Warm winds from the Pacific caused extensive Arctic sea-ice melt in summer 2007. *Climate Dyn.*, **36**, 2103–2112, https://doi.org/10.1007/s00382-010-0809-z.

——, P. L. Langen, and T. Mauritsen, 2014: Polar amplification in CCSM4: Contributions from the lapse rate and surface albedo feedbacks. *J. Climate*, **27**, 4433–4450, https://doi.org/10.1175/JCLI-D-13-00551.1.

Groves, D. G., and J. A. Francis, 2002: Moisture budget of the Arctic atmosphere from TOVS satellite data. *J. Geophys. Res.*, **107**, 4391, https://doi.org/10.1029/2001JD001191.

Hall, A., 2004: The role of surface albedo feedback in climate. *J. Climate*, **17**, 1550–1568, https://doi.org/10.1175/1520-0442(2004)017<1550:TROSAF>2.0.CO;2.

Hansen, J., M. Sato, and R. Ruedy, 1997: Radiative forcing and climate response. *J. Geophys. Res.*, **102**, 6831–6864, https://doi.org/10.1029/96JD03436.

——, and Coauthors, 2005: Efficacy of climate forcings. *J. Geophys. Res.*, **110**, D18104, https://doi.org/10.1029/2005JD005776.

——, M. Sato, R. Ruedy, K. Lo, D. W. Lea, and M. Medina-Elizade, 2006: Global temperature change. *Proc. Natl. Acad. Sci. USA*, **103**, 14 288–14 293, https://doi.org/10.1073/pnas.0606291103.

Hassol, S., 2004: *Impacts of a Warming Arctic—Arctic Climate Impact Assessment*. Cambridge University Press, 139 pp.

Held, I. M., and B. J. Soden, 2006: Robust responses of the hydrological cycle to global warming. *J. Climate*, **19**, 5686–5699, https://doi.org/10.1175/JCLI3990.1.

Hwang, Y. T., D. M. Frierson, and J. E. Kay, 2011: Coupling between Arctic feedbacks and changes in poleward energy transport. *Geophys. Res. Lett.*, **38**, L17704, https://doi.org/10.1029/2011GL048546.

IPCC, 2014: *Climate Change 2014: Impacts, Adaptation, and Vulnerability. Part B: Regional Aspects*. Cambridge University Press, 688 pp., http://www.ipcc.ch/pdf/assessment-report/ar5/wg2/WGIIAR5-PartB_FINAL.pdf.

Kang, S. M., and S.-P. Xie, 2014: Dependence of climate response on meridional structure of external thermal forcing. *J. Climate*, **27**, 5593–5600, https://doi.org/10.1175/JCLI-D-13-00622.1.

——, I. M. Held, D. M. Frierson, and M. Zhao, 2008: The response of the ITCZ to extratropical thermal forcing: Idealized slab-ocean experiments with a GCM. *J. Climate*, **21**, 3521–3532, https://doi.org/10.1175/2007JCLI2146.1.

——, K. Park, F. F. Jin, and M. F. Stuecker, 2017: Common warming pattern emerges irrespective of forcing location. *J. Adv. Model. Earth Syst.*, **9**, 2413–2424, https://doi.org/10.1002/2017MS001083.

Kapsch, M.-L., R. G. Graversen, and M. Tjernström, 2013: Springtime atmospheric energy transport and the control of Arctic summer sea-ice extent. *Nat. Climate Change*, **3**, 744–748, https://doi.org/10.1038/nclimate1884.

Kay, J. E., M. M. Holland, C. M. Bitz, E. Blanchard-Wrigglesworth, A. Gettelman, A. Conley, and D. Bailey, 2012: The influence of local feedbacks and northward heat transport on the equilibrium Arctic climate response to increased greenhouse gas forcing. *J. Climate*, **25**, 5433–5450, https://doi.org/10.1175/JCLI-D-11-00622.1.

Lu, J., and M. Cai, 2009: Seasonality of polar surface warming amplification in climate simulations. *Geophys. Res. Lett.*, **36**, L16704, https://doi.org/10.1029/2009GL040133.

Manabe, S., 1983: Carbon dioxide and climatic change. *Advances in Geophysics*, Vol. 25, Academic Press, 39–82, https://doi.org/10.1016/S0065-2687(08)60171-5.

Pithan, F., and T. Mauritsen, 2014: Arctic amplification dominated by temperature feedbacks in contemporary climate models. *Nat. Geosci.*, **7**, 181–184, https://doi.org/10.1038/ngeo2071.

Polyakov, I. V., and Coauthors, 2002: Observationally based assessment of polar amplification of global warming. *Geophys. Res. Lett.*, **29**, 1878, https://doi.org/10.1029/2001GL011111.

Rodgers, K. B., G. Lohmann, S. Lorenz, R. Schneider, and G. M. Henderson, 2003: A tropical mechanism for Northern Hemisphere deglaciation. *Geochem. Geophys. Geosyst.*, **4**, 1046, https://doi.org/10.1029/2003GC000508.

Rose, B. E., K. C. Armour, D. S. Battisti, N. Feldl, and D. D. Koll, 2014: The dependence of transient climate sensitivity and radiative feedbacks on the spatial pattern of ocean heat uptake. *Geophys. Res. Lett.*, **41**, 1071–1078, https://doi.org/10.1002/2013GL058955.

Rothrock, D., J. Zhang, and Y. Yu, 2003: The arctic ice thickness anomaly of the 1990s: A consistent view from observations and models. *J. Geophys. Res.*, **108**, 3083, https://doi.org/10.1029/2001JC001208.

Schneider, E. K., R. S. Lindzen, and B. P. Kirtman, 1997: A tropical influence on global climate. *J. Atmos. Sci.*, **54**, 1349–1358, https://doi.org/10.1175/1520-0469(1997)054<1349:ATIOGC>2.0.CO;2.

Schweiger, A. J., R. W. Lindsay, S. Vavrus, and J. A. Francis, 2008: Relationships between Arctic sea ice and clouds during autumn. *J. Climate*, **21**, 4799–4810, https://doi.org/10.1175/2008JCLI2156.1.

Screen, J. A., C. Deser, and I. Simmonds, 2012: Local and remote controls on observed Arctic warming. *Geophys. Res. Lett.*, **39**, L10709, https://doi.org/10.1029/2012GL051598.

Sellers, W. D., 1969: A global climatic model based on the energy balance of the earth-atmosphere system. *J. Appl. Meteor.*, **8**, 392–400, https://doi.org/10.1175/1520-0450(1969)008<0392:AGCMBO>2.0.CO;2.

Seo, J., S. M. Kang, and D. M. Frierson, 2014: Sensitivity of intertropical convergence zone movement to the latitudinal position of thermal forcing. *J. Climate*, **27**, 3035–3042, https://doi.org/10.1175/JCLI-D-13-00691.1.

Serreze, M. C., and J. A. Francis, 2006: The Arctic amplification debate. *Climatic Change*, **76**, 241–264, https://doi.org/10.1007/s10584-005-9017-y.

Simmonds, I., C. Burke, and K. Keay, 2008: Arctic climate change as manifest in cyclone behavior. *J. Climate*, **21**, 5777–5796, https://doi.org/10.1175/2008JCLI2366.1.

Stroeve, J., M. M. Holland, W. Meier, T. Scambos, and M. Serreze, 2007: Arctic sea ice decline: Faster than forecast. *Geophys. Res. Lett.*, **34**, L09501, https://doi.org/10.1029/2007GL029703.

Winton, M., 2006: Amplified Arctic climate change: What does surface albedo feedback have to do with it? *Geophys. Res. Lett.*, **33**, L03701, https://doi.org/10.1029/2005GL025244.

Yang, X. Y., J. C. Fyfe, and G. M. Flato, 2010: The role of poleward energy transport in Arctic temperature evolution. *Geophys. Res. Lett.*, **37**, L14803, https://doi.org/10.1029/2010GL043934.

Yoshimori, M., A. Abe-Ouchi, M. Watanabe, A. Oka, and T. Ogura, 2014: Robust seasonality of Arctic warming processes in two different versions of the MIROC GCM. *J. Climate*, **27**, 6358–6375, https://doi.org/10.1175/JCLI-D-14-00086.1.

——, ——, and A. Laîné, 2017: The role of atmospheric heat transport and regional feedbacks in the Arctic warming at equilibrium. *Climate Dyn.*, **49**, 3457–3472, https://doi.org/10.1007/s00382-017-3523-2.

Zhang, X., J. E. Walsh, J. Zhang, U. S. Bhatt, and M. Ikeda, 2004: Climatology and interannual variability of Arctic cyclone activity: 1948–2002. *J. Climate*, **17**, 2300–2317, https://doi.org/10.1175/1520-0442(2004)017<2300:CAIVOA>2.0.CO;2.